Error estimation and adaptive mesh refinement for aerodynamic flows

Ralf Hartmann, Joachim Held, Tobias Leicht and Florian Prill

Abstract We consider the adjoint-based error estimation and goal-oriented mesh refinement for single and multiple aerodynamic force coefficients as well as residual-based mesh refinement applied to various three-dimensional laminar and turbulent aerodynamic test cases defined in the ADIGMA project.

1 Introduction

Important quantities in aerodynamic flow simulations are the aerodynamic force coefficients like the drag, lift and moment coefficients. In addition to the exact approximation of these quantities it is of increasing importance, in particular in the field of uncertainty quantification, to estimate the error in the computed quantities. By employing a duality argument error estimates can be derived for estimating the error measured in terms of the aerodynamic force coefficients. The error estimate includes primal residuals multiplied by the solution to an adjoint problem related to the force coefficient. The error estimate can be decomposed into a sum of local adjoint-based indicators which can be employed to drive a goal-oriented adaptive mesh refinement algorithm specifically tailored to the accurate and efficient approximation of the aerodynamic force coefficient.

Provided the adjoint solution related to an arbitrary target functional is sufficiently smooth the corresponding error representation can be bounded from above by an error estimate which includes primal residuals but is independent of the adjoint solution. By localizing this error estimate so-called residual-based indicators are obtained. Mesh refinement based on these indicators leads to meshes which resolve *all* flow features irrespective of any specific target quantity.

Institute of Aerodynamics and Flow Technology, DLR (German Aerospace Center), Lilienthalplatz 7, 38108 Braunschweig, Germany, e-mail: Ralf.Hartmann@dlr.de

Before the start of the ADIGMA project the techniques of error estimation, adjoint-based mesh refinement and residual-based mesh refinement were available for 2d laminar compressible flows around simple airfoil geometries, see e.g. [5, 11]. Within the ADIGMA project these techniques have been extended to 3d laminar compressible flows, see [13], as well as to 2d turbulent and 3d turbulent compressible flows. Furthermore, the error estimation and adjoint-based mesh refinement for single target quantities has been extended to the treatment of multiple target quantities, see [6]. The algorithms are applied to a range of test cases defined in the ADIGMA project.

2 Error estimation and adaptive mesh refinement

We consider the discontinuous Galerkin (DG) finite element discretization of the compressible flow equations, see e.g. [12, 13]: Find $\mathbf{u}_h \in \mathbf{V}_{h,p}$ such that

$$\mathcal{N}(\mathbf{u}_h, \mathbf{v}_h) = 0 \qquad \forall \mathbf{v}_h \in \mathbf{V}_{h,p}, \tag{1}$$

where the discrete function space $\mathbf{V}_{h,p}$ consists of discontinuous piecewise polynomial functions of degree $p \geq 0$. Given a target quantity $J(\mathbf{u})$ like for example the aerodynamic drag, lift or moment coefficient, a duality argument can be employed, see e.g. [3, 9], to obtain following error representation

$$J(\mathbf{u}) - J(\mathbf{u}_h) = -\mathcal{N}(\mathbf{u}_h, \mathbf{z} - \mathbf{z}_h) \equiv \mathcal{R}(\mathbf{u}_h, \mathbf{z} - \mathbf{z}_h) \approx \mathcal{R}(\mathbf{u}_h, \tilde{\mathbf{z}}_h - \mathbf{z}_h) \tag{2}$$

for any discrete function $\mathbf{z}_h \in \mathbf{V}_{h,p}$, where the exact adjoint solution $\mathbf{z}$ is replaced by the solution $\tilde{\mathbf{z}}_h$ to following discrete adjoint problem: Find $\tilde{\mathbf{z}}_h \in \tilde{\mathbf{V}}_{h,p}$ such that

$$\mathcal{N}'[\mathbf{u}_h](\mathbf{w}_h, \tilde{\mathbf{z}}_h) = J'[\mathbf{u}_h](\mathbf{w}_h) \quad \forall \mathbf{w}_h \in \tilde{\mathbf{V}}_{h,p}. \tag{3}$$

A possible choice of the adjoint discrete function space is $\tilde{\mathbf{V}}_{h,p} = \mathbf{V}_{h,p+1}$. The approximate error representation in (2) can be localized

$$J(\mathbf{u}) - J(\mathbf{u}_h) \approx \mathcal{R}(\mathbf{u}_h, \tilde{\mathbf{z}}_h - \mathbf{z}_h) \equiv \sum_{\kappa \in \mathcal{T}_h} \tilde{\eta}_\kappa, \tag{4}$$

where $\tilde{\eta}_\kappa$ are the so-called *adjoint-based indicators* which include the local residuals multiplied by the discrete adjoint solution. These indicators can be used to drive an adaptive mesh refinement algorithm tailored to the accurate and efficient approximation of the target quantity $J(\mathbf{u})$ under consideration.

The extension of the adjoint-based error estimation and mesh refinement approach to multiple target quantities has previously been considered for the inviscid Burgers' equation in [10] and has been extended within the ADIGMA project to viscous compressible flows in [6]. Estimating the error in multiple

quantities of interest, $J_i(\mathbf{u}), i = 1, \ldots, N$, would require the computation of the solutions $\tilde{\mathbf{z}}_{h,i} \in \tilde{\mathbf{V}}_{h,p}$ to N discrete adjoint problems:

$$\mathcal{N}'[\mathbf{u}_h](\mathbf{w}_h, \tilde{\mathbf{z}}_{h,i}) = J_i'[\mathbf{u}_h](\mathbf{w}_h) \quad \forall \mathbf{w}_h \in \tilde{\mathbf{V}}_{h,p}, \quad i = 1, \ldots, N, \tag{5}$$

and the evaluatation of the error representation for each of the quantities,

$$J(\mathbf{u}) - J(\mathbf{u}_h) \approx \mathcal{R}(\mathbf{u}_h, \tilde{\mathbf{z}}_{h,i} - \mathbf{z}_{h,i}), \quad i = 1, \ldots, N. \tag{6}$$

Instead, we compute the solution to following discrete error equation,

$$\mathcal{N}'[\mathbf{u}_h](\tilde{\mathbf{e}}_h, \mathbf{w}_h) = \mathcal{R}(\mathbf{u}_h, \mathbf{w}_h) \quad \forall \mathbf{w}_h \in \tilde{\mathbf{V}}_{h,p}, \tag{7}$$

and evaluate following approximation of $J_i(\mathbf{u}) - J_i(\mathbf{u}_h)$,

$$J_i(\mathbf{u}) - J_i(\mathbf{u}_h) \approx J_i'[\mathbf{u}_h](\mathbf{e}) \approx J_i'[\mathbf{u}_h](\tilde{\mathbf{e}}_h), \quad i = 1, \ldots, N, \tag{8}$$

where $\mathbf{e} = \mathbf{u} - \mathbf{u}_h$. Furthermore, defining a suitable combination $J_c(\mathbf{u})$ of the original target quantities, see [6], we compute the solution to following discrete adjoint problem

$$\mathcal{N}'[\mathbf{u}_h](\mathbf{w}_h, \tilde{\mathbf{z}}_{c,h}) = J_c'[\mathbf{u}_h](\mathbf{w}_h) \quad \forall \mathbf{w}_h \in \tilde{\mathbf{V}}_{h,p}, \tag{9}$$

and evaluate the error estimate

$$J_c(\mathbf{u}) - J_c(\mathbf{u}_h) = \mathcal{R}(\mathbf{u}_h, \mathbf{z}_c - \mathbf{z}_h) \approx \mathcal{R}(\mathbf{u}_h, \tilde{\mathbf{z}}_{c,h} - \mathbf{z}_h) \equiv \sum_{\kappa \in \mathcal{T}_h} \tilde{\eta}_\kappa^c. \tag{10}$$

The combined target quantity $J_c(\mathbf{u})$ can be defined, see [6], such that the error with respect to $J_c(\cdot)$ represents the sum of relative errors in the original target quantities, $\sum_{i=1}^N |J_i(\mathbf{u}) - J_i(\mathbf{u}_h)|/|J_i(\mathbf{u}_h)|$, or a weighted sum of absolute errors, $\sum_{i=1}^N \alpha_i |J_i(\mathbf{u}) - J_i(\mathbf{u}_h)|$ with weighting factors $\alpha_i > 0$. The adjoint-based indicators, $\tilde{\eta}_\kappa^c$, obtained by localizing the estimate (10) can be used to drive an adaptive algorithm for the accurate and efficient approximation of all the target quantities, $J_i(\mathbf{u}), i = 1, \ldots, N$, under consideration.

Finally, we note that for a target quantity $J(\mathbf{u})$ with a sufficiently smooth adjoint solution the error representation (2) can be bounded from above as follows

$$|J(\mathbf{u}) - J(\mathbf{u}_h)| \leq \left(\sum_{\kappa \in \mathcal{T}_h} (\eta_\kappa^{\mathrm{res}})^2 \right)^{1/2}, \tag{11}$$

see [6, 8, 11, 13], where the so-called *residual-based indicators* $\eta_\kappa^{\mathrm{res}}$ include the primal residuals but are independent of the adjoint solution. Not depending on a particular target quantity the mesh refinement using residual-based indicators targets at resolving all flow features.

3 Numerical results

In this section we demonstrate the performance of the adjoint-based error estimation, the goal-oriented and the residual-based mesh refinement for a range of aerodynamic test cases defined in the ADIGMA project. The computations have been performed with the DLR PADGE code [7] which is based on a modified version of the `deal.II` library [1].

3.1 ADIGMA BTC3: Laminar flow around delta wing

First we consider a laminar flow around a delta wing. The delta wing has a sharp leading edge and a blunt trailing edge. A similar case has previously been considered in [15]. The geometry of the delta wing can be seen from the initial surface mesh in Figure 1(a). The delta wing is considered at laminar

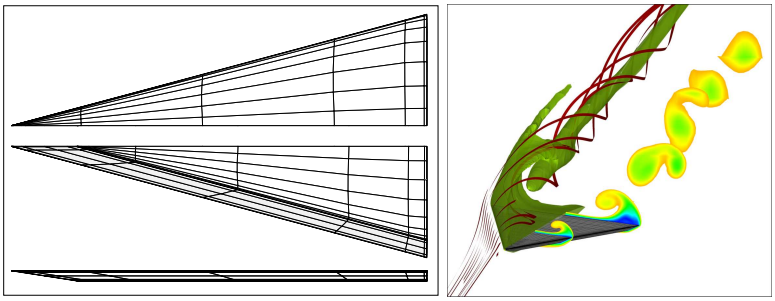

(a) (b)

Fig. 1 Laminar delta wing: a) initial surface mesh: Top, bottom and side view of the half delta wing with straight leading edges, b) solution plot showing streamlines and a Mach number isosurface over the left half of the wing as well as Mach number slices over the right half, [13].

conditions with inflow Mach number equal to 0.3, at an angle of attack $\alpha = 12.5°$, and Reynolds number $\mathrm{Re} = 4000$ with isothermal no-slip wall boundary condition imposed on the wing geometry. As the flow passes the leading edge it rolls up, creates a vortex and a secondary vortex. The resulting vortex system remains over long distances behind the wing, see Figure 1(b). In the following the total drag, lift, and moment coefficients, C_d, C_l and C_m, will be computed up to a predefined error tolerance `TOL`. The following industrial accuracy requirements have been defined:

$$\begin{aligned} |J_{C_\mathrm{l}}(\mathbf{u}) - J_{C_\mathrm{l}}(\mathbf{u}_h)| &\leq \mathtt{TOL}_{C_\mathrm{l}} = 10^{-2}, \\ |J_{C_\mathrm{d}}(\mathbf{u}) - J_{C_\mathrm{d}}(\mathbf{u}_h)| &\leq \mathtt{TOL}_{C_\mathrm{d}} = 10^{-3}, \\ |J_{C_\mathrm{m}}(\mathbf{u}) - J_{C_\mathrm{m}}(\mathbf{u}_h)| &\leq \mathtt{TOL}_{C_\mathrm{m}} = 10^{-3}. \end{aligned} \tag{12}$$

By performing high order computations on fine meshes the following reference values of the force coefficients have been obtained: $J_{C_\mathrm{l}}(\mathbf{u}) = C_\mathrm{l}^\mathrm{ref} = 0.34865$, $J_{C_\mathrm{d}}(\mathbf{u}) = C_\mathrm{d}^\mathrm{ref} = 0.16608$, and $J_{C_\mathrm{m}}(\mathbf{u}) = C_\mathrm{m}^\mathrm{ref} = -0.03065$.

In the following we compare the performance of various refinement strategies in meeting these accuracy requirements. In particular, we consider the single-target error estimation and mesh refinement approach for each of the C_l, C_d, and C_m coefficients, separately. This results in three different sequences of locally refined meshes where on each mesh a flow problem (1) and a discrete adjoint problem (3) are solved and the error estimate (4) is evaluated. This is compared to residual-based and to global mesh refinement. Furthermore, we consider a multi-target error estimation and mesh refinement approach for reducing the sum of relative errors of the C_l, C_d and C_m coefficients. This results in one sequence of locally refined meshes which is targeted at reducing the error in all three coefficients, simultaneously. Here, on each mesh a flow problem (1), a discrete error equation (7), and a discrete adjoint problem (9) are solved and the error estimates (8) and (10) are evaluated.

In Figure 2(a)-(c) we see that for C_l and C_d the residual-based refinement is more efficient than global mesh refinement which, however, is not the case for C_m. Whereas the residual-based indicators target at resolving all flow features, see the resolution of the vortex system in Fig. 3, they do not necessarily result in meshes suitable for accurately approximating force coefficients. In contrast to that we see that the adjoint-based refinement is significantly more accurate than both, residual-based and global mesh refinement. Furthermore, we see that the accuracy of the single-target and the multi-target adjoint-based mesh refinement is comparable. Finally, we see that the enhanced force coefficients, $\tilde{C}_\mathrm{d/l/m} = C_\mathrm{d/l/m} + \sum_{\kappa\in\mathcal{T}_h} \tilde{\eta}_\kappa$, in case of the single-target algorithm and $\tilde{C}_\mathrm{d/l/m} = C_\mathrm{d/l/m} + J_i'[\mathbf{u}_h](\tilde{\mathbf{e}}_h)$ in case of the multi-target algorithm, are significantly more accurate than the original $C_\star$ values on the adjoint-based refined meshes. This demonstrates that the error estimation for single as well as for multiple target quantities is accurate and reliable.

Figure 2(d) shows the error in the drag coefficient vs. the computing time relative to the extrapolated time required for global mesh refinement to meet the tolerances (12). For meeting the tolerances (12) the residual-based mesh refinement requires about 10% of the time required for global mesh refinement. The adjoint-based mesh refinement requires about 2% and the adjoint-based mesh refinement including error estimation requires in the range of 0.1%. These time measurements include the time for solving the flow problem and possibly the adjoint problem and the discrete error accumulated for the solutions on coarser meshes. The time comparison clearly demonstrates the advantage of using error estimation and adjoint-based mesh refinement.

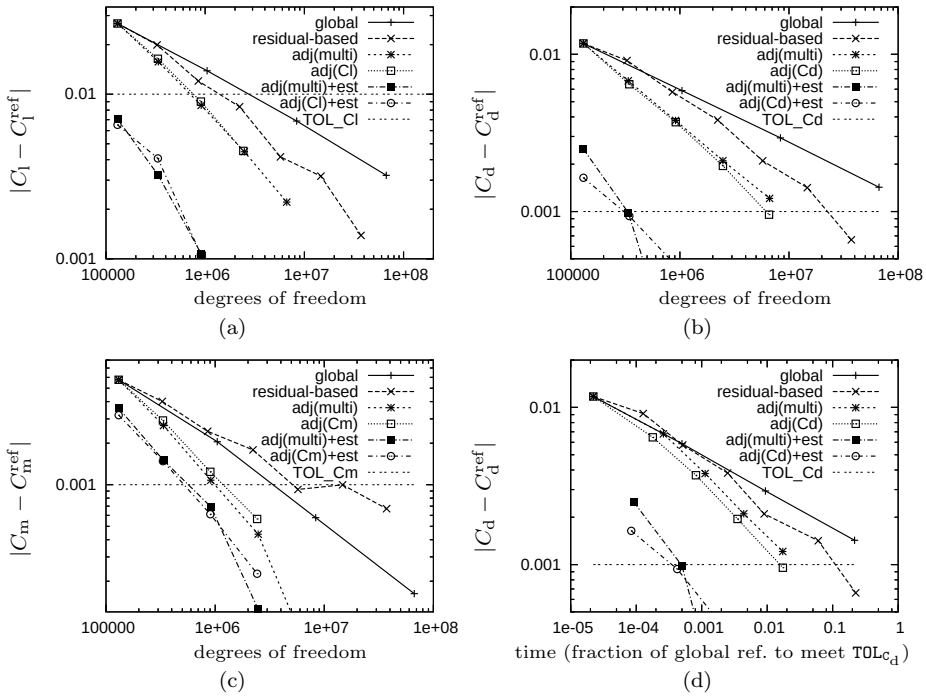

Fig. 2 Error in the (a) lift, (b) drag, and (c) moment coefficient for global, residual-based, adjoint-based(single-target) and adjoint-based(multi-target) mesh refinement vs. number of degrees of freedom. On the adjoint-based refined meshes also the enhanced coefficients $\tilde{C}_{l/d/m} = C_{l/d/m} + \text{est.}$ are given. (d) Error in the drag vs. computing time relative to the extrapolated time required for global mesh refinement to meet the tolerances (12).

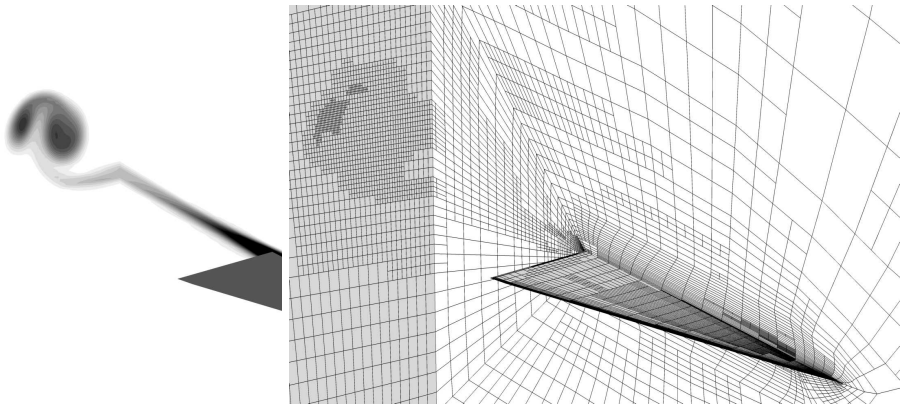

Fig. 3 (a) Mach number isolines of flow solution on (b) the last but one residual-based refined mesh.

3.2 ADIGMA BTC1: L1T2 high-lift configuration

In this section we consider a turbulent flow around the L1T2 three-element airfoil, see Fig. 5(a), at a Mach number $M = 0.197$, a Reynolds number $Re = 3.52 \cdot 10^6$ and an angle of attack $\alpha = 20.18°$. This case has been documented extensively in the literature, see e. g. [4, 14]. In particular, there is data of two wind tunnel experiments (experiment 1 & 2) available, see [16].

A DG discretization of the RANS-$k\omega$ equations is used which represents a slight modification of the BR2 scheme proposed in [2]. Menter's wall boundary condition is used, where the first wall boundary layer grid spacing y_1 is chosen such that y_1^+ is in the range of one.

First, we compare numerical results generated by the PADGE code with results generated by the well validated finite volume code TAU [17] as well as with experimental data. The PADGE computations were performed with polynomial degrees $p = 3$ and $p = 4$, each on the same quadrilateral mesh with 4 740 curved elements, see Figure 4. This mesh emerged from an original 75 840 element mesh by two agglomeration steps. The curved mesh representation in this case is realized by piecewise polynomials of degree 4 based on additional points which have been extracted from the original mesh.

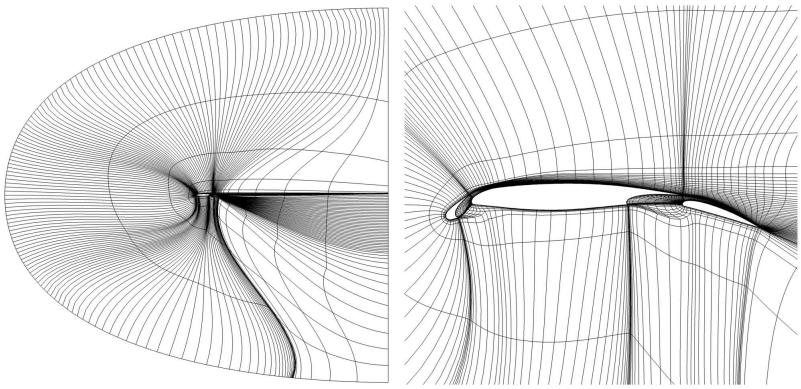

Fig. 4 L1T2 high lift configuration: Coarse grid of 4 740 curved elements.

Figure 5(b) shows the pressure distribution over each of the airfoil elements, i.e., slat, main element and flap. Here, we see that the output by the PADGE code is in good agreement with the experimental data and with only minor differences compared to the TAU reference results. Furthermore, Figure 6 shows the comparison for the skin friction distribution. Whereas there are still considerable differences between the computed skin friction distribution for $p = 3$, the result for $p = 4$ is overall in good agreement with the TAU reference computation. We note that with a polynomial degree $p = 4$ on cells near the wall boundary and $p = 3$ everywhere else the c_p and c_f distributions were almost identical to that with the globally high $p = 4$ polynomials. The

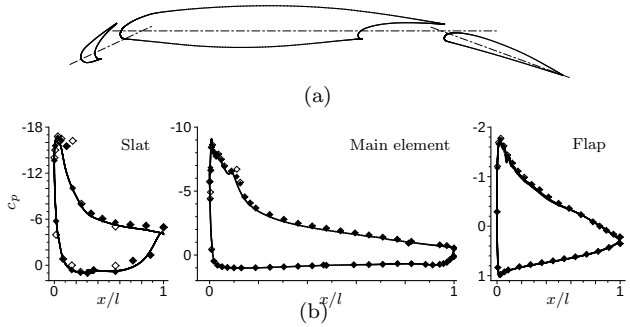

Fig. 5 a) Geometry of the L1T2 three-element airfoil. b) Pressure distributions for each L1T2 airfoil element computed by PADGE (solid line) compared to reference results by TAU (dotted) and data of experiment 1 (open symbols) and experiment 2 (filled), [7].

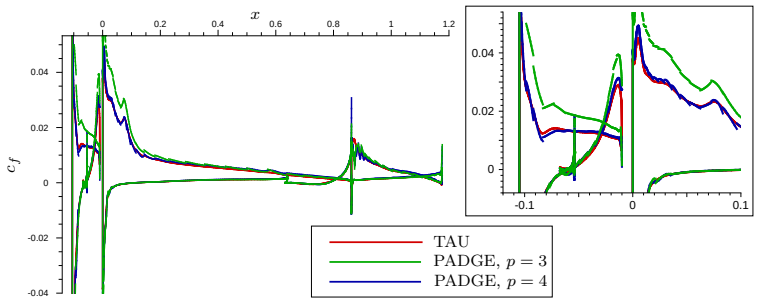

Fig. 6 L1T2 three-element airfoil. Comparison of computed skin friction distributions with details of the slat region, [7].

$p = 4$ solution has almost as many degrees of freedom as the computation with the TAU code on the original mesh with 75 840 elements and required about the same computing time as the TAU code.

In the following, we investigate the performance of the adjoint-based error estimation and mesh refinement for this test case. Starting with a $p = 1$ solution on the coarse mesh of 4 740 curved elements, we consider the adjoint-based refinement targeted at efficiently approximating the drag coefficient C_{d}. In Figure 7(a) we compare the convergence of C_{d} for the global and the adjoint-based mesh refinement. We see that with the adjoint-based refinement the C_{d} value converges significantly faster to the C_{d} reference value than with global mesh refinement. Furthermore, we see that using the error estimation on the adjoint-based refined meshes for computing enhanced drag coefficients $\tilde{C}_{\mathrm{d}}$ further improves the C_{d} value which demonstrates that the error estimation is accurate and reliable. Figure 7(b) shows a zoom of the final adjoint-based refined mesh. We see that the mesh has been refined in the neighborhood of the line which separates the recirculation zone behind the slat from the flow which passes between the slat and the main element.

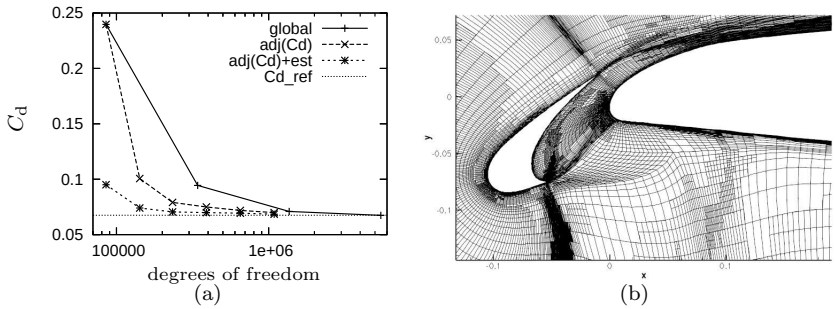

Fig. 7 L1T2 high lift configuration: (a) drag, C_{d}, coefficient values on globally and adjoint-based refined meshes; on the latter also the enhanced $\tilde{C}_{\mathrm{d}}$ values are given; (b) Zoom of the adjoint-based refined mesh.

There is some refinement in the wake of the slat. Furthermore, the mesh has been refined in the neighborhood of the stagnation streamline of the main element. We note that, similarly, the stagnation streamlines of the slat and flap are refined. Here, the adjoint solution indicates that the exact position of the stagnation points, as well as the flow upstream of them is particularly important for an accurate prediction of the drag coefficient.

3.3 ADIGMA BTC0: Turbulent flow around a streamlined body

We consider a turbulent flow around a streamlined body at a Mach number $M = 0.5$, an angle of attack $\alpha = 5°$, and a Reynolds number $\mathrm{Re} = 10 \cdot 10^6$ with adiabatic noslip wall boundary conditions. Reference values $J_{C_{\mathrm{l}}}(\mathbf{u}) = 0.006612$ and $J_{C_{\mathrm{d}}}(\mathbf{u}) = 0.0085646$ have been obtained based on higher order computations on very fine grids. The starting mesh of this computation, see Figure 9(a), has 6 656 curved elements. The edges are given by polynomials of degree 4 created by taking additional points from the nested finer grids.

In Figure 8(a) we compare the convergence of C_{l} for global, residual-based and adjoint-based mesh refinement. We see that within the first refinement step the C_{l} value for the adjoint-based refinement converges as fast as for the residual-based refinement but both significantly faster than global mesh refinement. However, from the second refinement step onwards the C_{l} values for the adjoint-based mesh refinement are significantly more accurate than for both residual-based and global mesh refinement. Furthermore, we see that the error estimation on the adjoint-based refined meshes further improves the C_{l} value. In fact, computing the flow solution and its adjoint on the coarsest mesh results in an enhanced $\tilde{C}_{\mathrm{l}}$ value which almost coincides with the reference value. Figure 8(b) shows the corresponding error plot. Here

we see that the enhanced C_l value already on the coarsest mesh is more accurate than the prescribed ADIGMA tolerance $\mathtt{TOL}_{C_\mathrm{l}} = 0.001$ and is even more accurate than the C_l value on the finest adjoint-based, residual-based and globally refined meshes. Also, we see that for a stricter convergence criterion, there is an increasing gain from using adjoint-based refinement in comparison to residual-based and global mesh refinement. Figures 8(a)&(b) show the corresponding plots for the C_d value. Here, we see that the enhanced C_d value meets the ADIGMA tolerance, $\mathtt{TOL}_{C_\mathrm{d}} = 0.0003$, already on the first adjoint-based refined mesh.

Finally, Figure 9(b) shows the final residual-based refined mesh and Figures 9(c) & (d) show the final adjoint-based refined meshes targeted at the accurate and efficient approximation of the C_l and C_d values, respectively. Here, we see that the adjoint-based refinement is mainly concentrated near the body; indeed, the wake is almost unresolved. This corresponds to the fact, that the flow solution in and near the boundary layer is significantly more important for obtaining accurate aerodynamic force coefficients than the flow solution in the wake. In contrast to that the residual-based indicator which is targeted at resolving all flow features also refines elements in the vicinity of the wake.

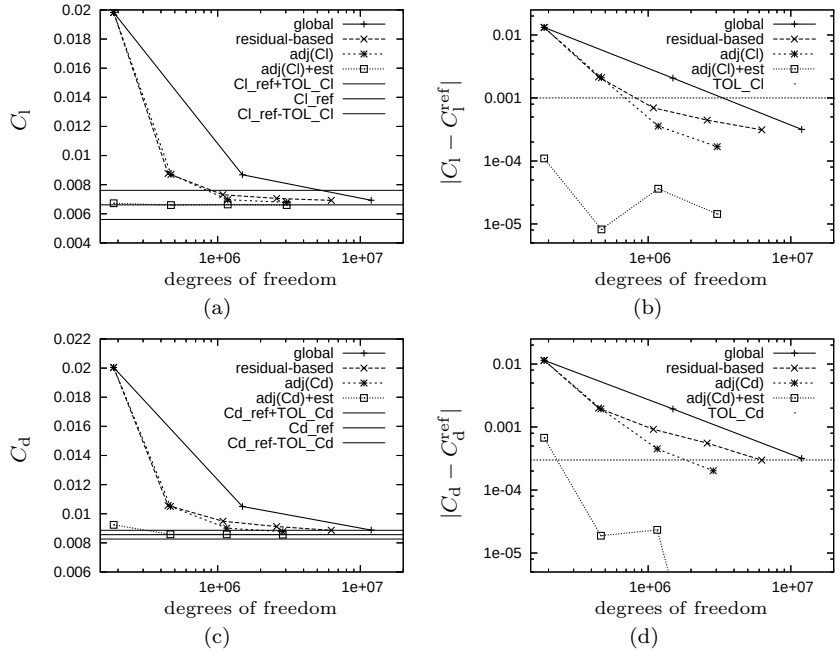

Fig. 8 ADGIMA BTC0 test case at turbulent conditions: (a) lift coefficients C_l on globally and residual-based refined meshes; C_l and the enhanced values, $\tilde{C}_\mathrm{l}$, on adjoint-based refined meshes vs. number of degrees of freedom; (b) the respective error plot. (c)&(d) the respective plots for the drag coefficient C_d.

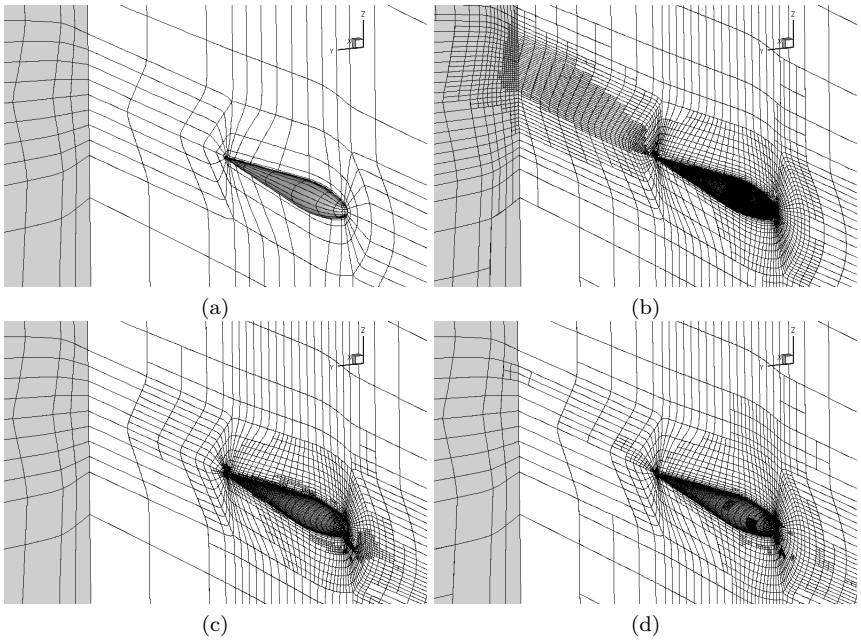

Fig. 9 ADGIMA BTC0 test case at turbulent conditions: (a) The coarse mesh with 6 656 curved elements. The edges are given by polynomials of degree 4. (b) Mesh after 4 residual-based refinement steps. (c)&(d) Meshes after 3 adjoint-based refinement steps targeted at C_l and C_d, respectively.

3.4 Subsonic turbulent flow around the DLR-F6 wing-body configuration

In this final example we consider a turbulent flow at Mach number $M = 0.5$, a Reynolds number $Re = 5 \cdot 10^6$ at an angle of attack $\alpha = -0.141$ around the DLR-F6 wing-body configuration without fairing. This is a modification of the drag prediction workshop (DPW) III test case. In fact, a fixed angle of attack has been assumed instead of a given target lift. Also, the Mach number has been reduced from originally $M = 0.75$ to $M = 0.5$ in order to ensure that the flow is subsonic. The original DPW mesh of 3.24 mio. hexahedral elements has been agglomerated twice resulting in a coarse mesh of 50 618 hexahedral elements. The additional points of the original mesh have been used to define 50 618 curved elements where the curved lines are represented by quartic polynomials. After some regularization this fifth order mesh has been used in a residual-based and an adjoint-based mesh refinement algorithm.

In Table 1 we collect the C_l and C_d values obtained by PADGE for the $p = 2, 3$ solutions on the coarsest and for the $p = 2$ solutions on a once globally

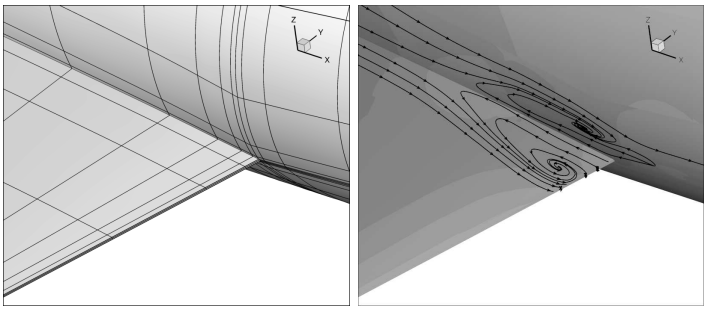

Fig. 10 DLR-F6 wing-body configuration: c_p distribution and wall stream lines of a 4^{th} order solution on the coarse mesh of 50 618 curved elements.

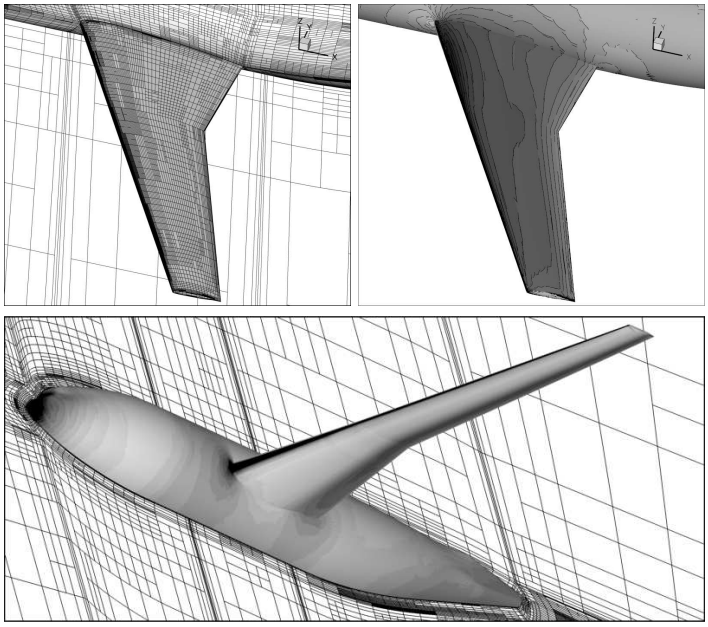

Fig. 11 DLR-F6 wing-body configuration: c_p distribution on mesh of 582 350 curved elements after 4 residual-based mesh refinement steps.

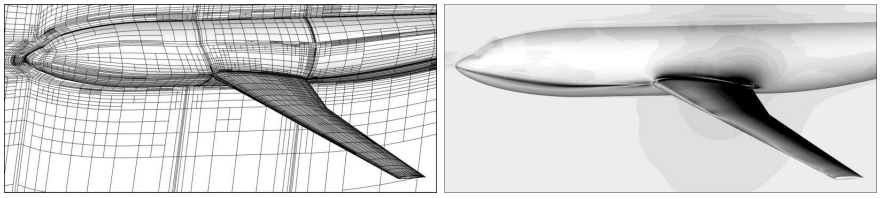

Fig. 12 DLR-F6 wing-body configuration: Density adjoint distribution, i.e., the first comp. of discrete adjoint solution $\tilde{\mathbf{z}}_h$ on a mesh of 202 314 curved elements after two adjoint-based mesh refinement steps targeted at C_l.

refined mesh in comparison with the values obtained by TAU on the original mesh. Figure 11 shows the surface mesh near the wing-body junction and the c_p distribution and wall stream lines of a 4^{th} order solution, i.e. for $p = 3$, on the coarse mesh. We clearly recognize a separation of the flow. Figure 11 shows the c_p distribution on a mesh of 582 350 curved elements after four anisotropic residual-based mesh refinement steps. Finally, Figure 12 shows an example of an adjoint-based refined mesh; here for the target quantity C_l, together with the adjoint solution connected to the C_l value.

	coarse mesh		once globally	original mesh
	$p = 2$	$p = 3$	refined, $p = 2$	TAU
C_l	0.424	0.413	0.416	0.423
C_d	0.0270	0.0251	0.0249	0.0237
C_m	-0.122	-0.121	-0.123	-0.125

Table 1 Subsonic turbulent flow around the DLR-F6 wing-body configuration: Comparison of force coefficients by the PADGE code [7] for $p = 2, 3$ and the TAU code [17].

4 Summary

Within the EU-project ADIGMA the techniques of error estimation, residual-based and adjoint-based mesh refinement have been extended from 2d laminar flows to 3d laminar and turbulent flows. They have been implemented in the PADGE code [7] and successfully applied to various aerodynamic test cases including a vortex dominated laminar flow around a delta wing, a turbulent flow around the L1T2 three-element high lift configuration and a turbulent flow around the DLR-F6 wing-body configuration. Furthermore, the error estimation and adjoint-based mesh refinement have been extended from single target quantities to the treatment of multiple target quantities.

The residual-based indicators which are targeted at resolving all flow features have been shown to well resolve vortical systems over long distances. Furthermore, it has been shown that using error estimation and adjoint-based mesh refinement the aerodynamic force coefficients can be approximated significantly more accurate and more efficient than with residual-based and global mesh refinement.

Current and future research is dedicated to extending the adaptation algorithms from isotropic to anisotropic mesh refinement [13] as well as to *hp*-refinement. The flow solver PADGE will be extended from purely hexahedral to hybrid meshes. Furthermore, a *p*-multilevel algorithm for 3d turbulent flows will be developed in order to replace the current implicit solver which relies on the storage of the full Jacobian matrix.

References

1. W. Bangerth, R. Hartmann, and G. Kanschat. deal.II – A general purpose object oriented finite element library. *ACM Trans. on Math. Software*, 33(4), Aug. 2007.
2. F. Bassi, A. Crivellini, S. Rebay, and M. Savini. Discontinuous Galerkin solution of the Reynolds-averaged Navier-Stokes and $k-\omega$ turbulence model equations. *Computers & Fluids*, 34:507–540, 2005.
3. R. Becker and R. Rannacher. An optimal control approach to a posteriori error estimation in finite element methods. *Acta Numerica*, 10:1–102, 2001.
4. I. Fejtek. Summary of code validation results for a multiple element airfoil test case. 28th AIAA fluid dynamics conference, 1997. AIAA Paper 97-1932.
5. R. Hartmann. Adaptive discontinuous Galerkin methods with shock-capturing for the compressible Navier-Stokes equations. *Int. J. Numer. Meth. Fluids*, 51(9–10):1131–1156, 2006.
6. R. Hartmann. Multitarget error estimation and adaptivity in aerodynamic flow simulations. *SIAM J. Sci. Comput.*, 31(1):708–731, 2008.
7. R. Hartmann, J. Held, T. Leicht, and F. Prill. Discontinuous Galerkin methods for computational aerodynamics – 3D adaptive flow simulation with the DLR PADGE code. *Aerospace Science and Technology*, 2009. Submitted.
8. R. Hartmann and P. Houston. Adaptive discontinuous Galerkin finite element methods for nonlinear hyperbolic conservation laws. *SIAM J. Sci. Comput.*, 24:979–1004, 2002.
9. R. Hartmann and P. Houston. Adaptive discontinuous Galerkin finite element methods for the compressible Euler equations. *J. Comput. Phys.*, 183(2):508–532, 2002.
10. R. Hartmann and P. Houston. Goal-oriented a posteriori error estimation for multiple target functionals. In T. Y. Hou and E. Tadmor, editors, *Hyperbolic problems: theory, numerics, applications*, pages 579–588. Springer, 2003.
11. R. Hartmann and P. Houston. Symmetric interior penalty DG methods for the compressible Navier–Stokes equations II: Goal–oriented a posteriori error estimation. *Int. J. Num. Anal. Model.*, 3(2):141–162, 2006.
12. R. Hartmann and P. Houston. An optimal order interior penalty discontinuous Galerkin discretization of the compressible Navier–Stokes equations. *J. Comput. Phys.*, 227(22):9670–9685, 2008.
13. R. Hartmann and T. Leicht. Error estimation and anisotropic mesh refinement for 3d aerodynamic flow simulations. *J. Comput. Phys.*, 2009. Submitted.
14. A. Hellsten. New Two-Equation Turbulence Model for Aerodynamics Applications. Technical Report Report No. A-21, Helsinki University of Technology, Laboratory of Aerodynamics, 2004.
15. C. M. Klaij, J. J. W. van der Vegt, and H. van der Ven. Space–time discontinuous Galerkin method for the compressible Navier-Stokes equations. *J. Comput. Phys.*, 217(2):589–611, 2006.
16. I. R. M. Moir. Measurements on a two-dimensional aerofoil with high-lift devices. AGARD Advisory Report 303, Advisory Group for Aerospace Research & Development, Neuilly-sur-Seine, 1994. Test case A2.
17. D. Schwamborn, T. Gerhold, and R. Heinrich. The DLR TAU-code: Recent applications in research and industry. In P. Wesseling, E. Oñate, and J. Périaux, editors, *Proceedings of European Conference on Computational Fluid Dynamics ECCOMAS CDF 2006, Delft The Netherland*, pages 91–100, 2006.